CHAPTER 5

Impact of E71S Mutation on SHANK3 Conformational Dynamics at the SPN-ARR Interface

Impact of E71S Mutation on SHANK3 Conformational Dynamics at the SPN-ARR Interface

5.1. Abstract:

Autism spectrum disorder (ASD) is a complicated neurological condition. The genetic factors implicated in ASD include a variety of loci that converge on neurological pathways, mainly excitatory synapses. SHANK3, a crucial protein in post-synaptic neuron cells, has been linked to ASD through mutations in the N-terminal, substantially the SPN domain. The purpose of this study is to evaluate the influence of the designed E71S mutation on SHANK3, assessing its dynamics, stability, flexibility, and compactness in comparison to the SHANK3 WT. Molecular dynamics simulations were employed to investigate the structural dynamics of both SHANK3 WT and the E71S mutant. The steps of simulation encompass heating dynamics, density equilibration, and production. Trajectory analysis included assessments of RMSD, RMSF, Rg, B-factor, hydrogen bond interactions, and changes in secondary structure.

The simulations unveiled that the E71S mutation perturbs the stability and folding of SHANK3, leading to the disturbance of intramolecular contacts between the SPN and ARR domains. The resulting disruption leads to an elevated separation between SPN and ARR domains, which may have implications for the protein's interactions with binding partners, such as αCaMKII and α-Fodrin. The modified conformation of the SPN-ARR tandem in the E71S mutant implies a potential influence on dendritic spine shape and plasticity of synaptic neurons.

SHANK3 E71S mutant hindered the stabilization and folding, disrupted intramolecular interactions between SPN and ARR domains, and decreased its binding with αCaMKII, whereas increased binding α-Fodrin to its sites on the SHANK3. These findings highlight its possible roles in neurodevelopmental disorders.

5.2. Introduction

Autism spectrum disorder (ASD) is a condition of neurological development that emerges during the first years of early childhood, characterized by an array of stereotyped activities, delays in communication, and social interaction disturbances [1]. The current worldwide incidence of ASD is estimated to be around 100 cases per 10,000

individuals [2]. A variety of genetic loci have been associated with the pathomechanisms of ASD. However, these loci ultimately lead to limited neural circuits that are involved in aberrant communication at excitatory synapses [3]. Consequently, one of the critical pathways underpinning the development of ASD has been postulated to be the alteration of post-synaptic neural excitation[4]. SHANK3 constitutes a crucial protein engaged in the post-synaptic density (PSD). SHANK3 was extensively investigated in nerve cells as a scaffolding protein [5]. Abnormal variations and dysregulation in SHANK3 have been linked to ASD [6-8]. SHANK3 encompasses five distinct domains. The Shank/ProSAP N-terminal (SPN) domain has a conformation that is similar to a ubiquitin-like (Ubl) domain, analogous to how Ras association domains. Previous research findings have established that activated Ras and Rap proteins exhibit elevated affinity to the SPN domain [9]. Furthermore, the SPN region bonds in close intramolecular interactions with the Ankyrin Repeat Region (ARR) or Ank domain, restricting accessibility of α-Fodrin and sharpin as known interaction partners of the Ank repeat [10]. Besides, the SH3 domain allows for interactions with AMPAR through GRIP. AMPARs, operating as ion channels, enhance fast synaptic communication and have impacts on cognitive processes, including learning and memory [11]. Moreover, within SHANK3, a proline-rich region is situated among the C-terminal SAM and PDZ domains [12]. Remarkably, point mutations have been spotlighted as prominent loci in the N-terminus [13]. Two autism-related mutations, R12C and L68P, in the SPN region impair SHANK3's interaction with Rap1, leading to a blockage in integrin activation.[14, 15]. Experimental findings indicate that the N52R mutation exposes the ARR region, facilitating subsequent binding to external GFP-SPN. Additionally, the N52R mutation either hinders or enhances SHANK3's functional role in actin binding, leading to changes in ASD-like symptoms controlled by SHANK3 *in vivo* [16]. A recent study postulated that N52R disruption of the interface of SPN−ARR caused a lack of αCaMKII ligating, which emerges to be a more common outcome of SHANK3 point variants. They hyposized a physiological impact of this connection might derive from the negative regulator actions of SHANK3 on the αCaMKII signaling pathway intensely engaged in synaptic plasticity [17].

The primary objective of the stated research is to create point mutation in the 71 position in the SPN region and investigate the impact of the SHANK3 point mutation E71S on synapse structure, function, and plasticity. To elucidate the intricate relationship between

genetic variations and the E71S mutant in comparison to SHANK3 wild type (WT) in the context of ASD pathogenesis, molecular dynamics (MD) simulations were employed. The stability of both SHANK3 WT and the SHANK3 E71S mutant structures was assessed, considering protein equilibrium, flexibility, and compactness. Subsequently, an evaluation was conducted to discern the potential effects of the deleterious mutation on protein binding sites, specifically those influencing neuronal transactions and synaptic plasticity.

5.3. Materials and Methods

5.3.1. Building of primary structures

5.3.1.1. SHANK3 protein

The SH3 and multiple ankyrin repeat domains 3 structure, PDB ID 5G4X [15], was downloaded from RCSB Protein Data Bank [18] and was utilized for molecular dynamics simulation.

5.3.1.2. Constructing the E71S SHANK3 mutant

The principal configuration of the E71S mutant was created by manipulating the three-dimensional configuration of the scaffold protein WT SHANK3 (PDB ID: 5G4X). The Rotamer tool of the CHIMERA program [19] was utilized to build E71S SHANK3, where Glutamic acid was substituted with Serine at nucleotide 71 in the SPN domain of SHANK3.

5.3.2. Setup for Molecular Dynamics simulations

SHANK3 E71S mutant and SHANK3 WT systems were constructed for the MD simulation utilizing ff99SBildn as a force field parameter in the Leap module of the AMBER 14 software package [20]. A prominent TIP3P water model [21] was applied as a solvent to explicitly stated SHANK3 WT and SHANK3 E71S mutant systems independently utilizing a buffer dimension of 10 Å in a periodic cubic box. The charge of the SHANK3 WT and the SHANK3 E71S mutant structures have been neutralized by the addition of an adequate number of counter ions and, afterwards, undergoing a reduction of energy to eliminate the London dispersion force.

The molecular dynamics simulation adheres to a consistent method comprising heating dynamics followed by density, equilibrium, and production dynamics. Initial structures

were energy-minimized for further Molecular Dynamics procedures. The gradual heating of structures from 0 to 300 K occurred under a steady volume (NVT) situation, followed by the density approach. Equilibration was accomplished under NPT conditions (300 K and 1 atm pressure) for one nanosecond. Visualization and analysis of energy, temperature, and pressure were undertaken to ensure correct equilibration. Subsequently, a 200 ns MD production run for stabilized structures using the PME algorithm [22, 23] with a time phase of 2 fs. A threshold of 8 Å addressed nonbonding connections, whereas electrostatic forces were managed using the PME technique. The SHAKE algorithm restricted all bonds [23], while temperature and pressure were maintained stationary via the Berendsen weak coupling algorithm over the simulation [24]. Snapshots were taken through the trajectory at intervals of 10 ns for further investigations of each structure.

The PTRAJ and CPPTRAJ modules of AmberTools 14 were applied to analyze molecular dynamics trajectories of both the SHANK3 WT and the SHANK3 E71S mutant [23] of AmberTools 14. To evaluate the convergent behavior of our structures, the RMSDs for SHANK3 WT and the SHANK3 E71S mutant have been analyzed, wherein the initial MD system was employed as the template for analysis.

Besides that, the two structures underwent Radius Gyration, hydrophobic interactions, and intramolecular distance analysis. The analysis of intra-molecular hydrogen bonds was performed for SHANK3 WT and the SHANK3 E71S mutant according to the potential donors (HD) and acceptors (HA) of the protons. UCSF Chimera software [19] was utilized to depict the 3D structure of each system. The xmgrace plotting tools were applied to generate the plots. The monitoring of pressure, temperature, kinetic energy, total energy, and potential energy was systematically validated throughout the simulation time for the SHANK3 WT and the SHANK3 E71S mutant systems.

5.3.3. Docking between the two structures and αCaMKII analysis

The docking between the two structures, SHANK3 WT and SHANK3 E71S mutant with protein partners αCaMKII and α-Fodrin, was conducted using a ClusPro (protein-protein docking) server, and the results were analyzed through the PDBsum server.

5.4. Results and Discussion

5.4.1. The root mean square deviation (RMSD)

RMSD analysis was carried out for a 200 ns simulation period comprising the SHANK3 WT protein and the SHANK3 E71S mutant. This analysis yielded crucial insights into their structural dynamics. RMSD of the SHANK3 WT protein exhibited a gradual rise with initial fluctuations, followed by a significant changeover at around 3.9 Å, and eventually stabilized towards the end of the simulation, as depicted in **Figures 5.1A** and **5.1B**. Conversely, the SHANK3 E71S mutant demonstrated an abrupt increase in impulse at 4.5 Å, followed by a reduction in RMSD and further fluctuations until the end of the simulation, as shown in **Figures 5.1C** and **5.1D**. The results indicate that the SHANK3 WT may exhibit greater stability than the SHANK3 E71S mutant, which could have increased structural flexibility.

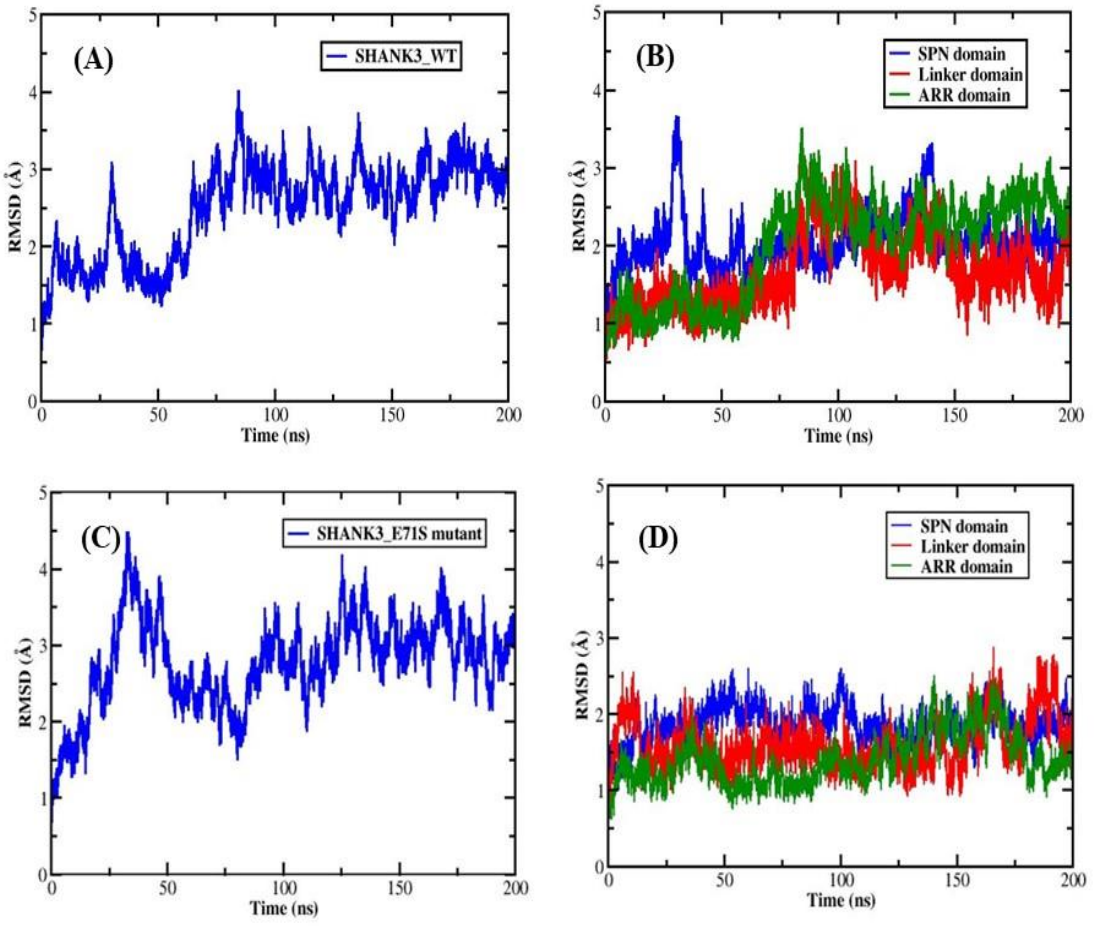

Figure 5.1 *The MD simulation analysis RMSD plot for (**A**) SHANK3 WT, (**B**) Three domains of SHANK3 WT, (**C**) SHANK3 E71S mutant, (**D**) Three domains of SHANK3 E71S mutant. The RMSD values exhibits in Angstrom are shown on the y-axis, while the x-axis exhibits the time.*

5.4.2. The root mean square Fluctuation (RMSF)

The findings of RMSF indicated marginally higher conformational flexibility in the SHANK3 WT, as illustrated in **Figures 5.2A** and **5.2B** comparison to the SHANK3 E71S mutant **Figures 5.2C** and **5.2D**. Noteworthy was the flexibility detected in amino acid residue corresponding to the position of the mutation of SHANK3 E71S mutant aligning with the SHANK3 SPN domain in the E71S mutant shown to be higher than in the SHANK3 WT protein. The SPN domain with high RMSF values might be functionally important. The influence of the E71S mutant on SHANK3 folding has been studied via the assessment of the Rg indicator.

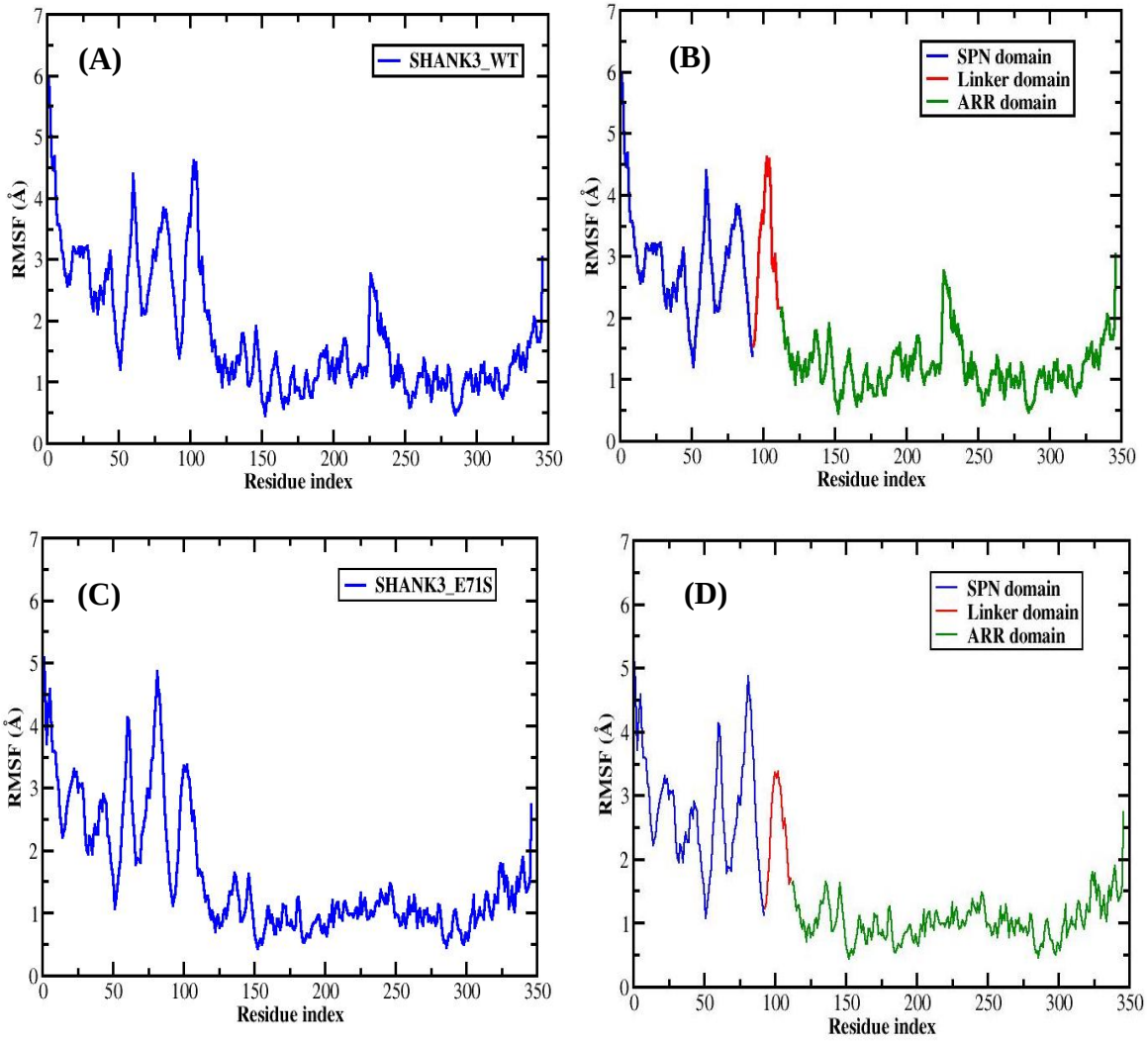

Figure 5.2 *The RMSF analysis plots (**A**) SHANK3 WT, (**B**) Three domains of SHANK3 WT, (**C**) SHANK3 E71S mutant, and (**D**) Three domains of SHANK3 E71S mutant.*

5.4.3. The radius of gyration (Rg) analysis

The radius of gyration (Rg) is a regularly adopted metric for evaluating the spatial distribution of atoms within a specific biological molecule computed from the principal center of gravity. The radius of gyration is applied to track changes in structural compactness and folded over simulation time. According to the Rg plots, the SHANK3 WT protein exposed lower values over time of the simulation of 200 ns, as exhibited in **Figure 5.3A**. Notably, the SHANK3 E71S mutant has elevated Rg values throughout the simulation **Figure 5.3B**; therefore, the SHANK3 E71S mutant relates to a less compact and unfolded state. To determine the constructional state between SPN and ARR domains, we apply the distance analysis between SPN and ARR domains.

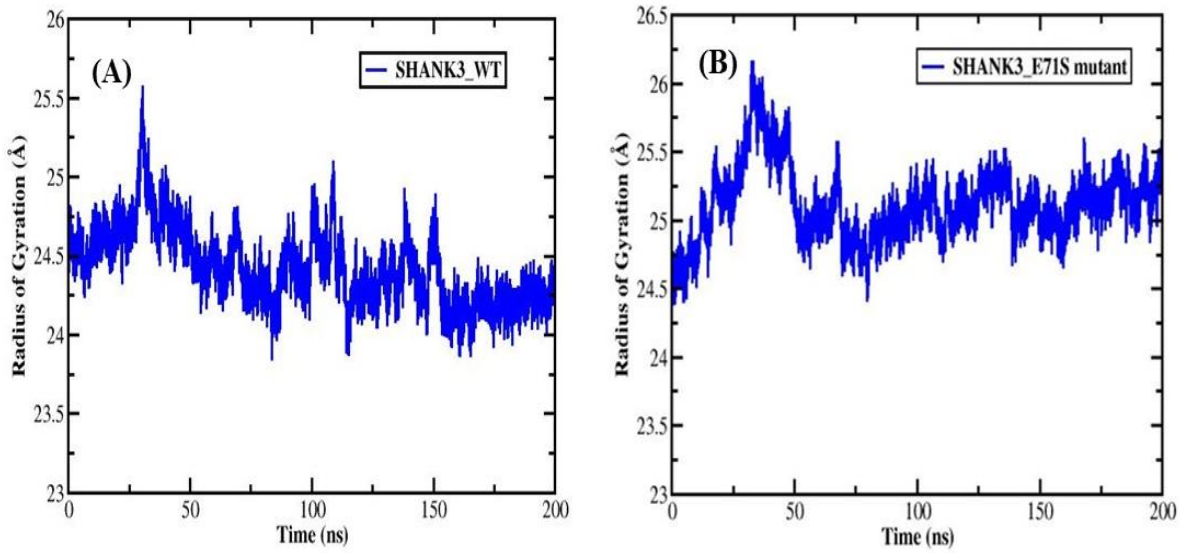

Figure 5.3 *The radius of gyration analysis Rg, (**A**) SHANK3 WT protein, (**B**) SHANK3 E71S mutant. The x-axis depicts the time ns, while the y-axis depicts the Radius gyration.*

5.4.4. Analysis of the distance between SPN and ARR domains

The central point of mass distance between the SPN-ARR domains of SHANK3 WT and the SHANK3 E71S mutant were evaluated. Initially, the distance between SPN-ARR in the SHANK3 WT protein increased, followed by a sudden reduction, and continued with a stabilization state to the end of the simulation (**Figure 5.4A**). Conversely, the SHANK3 E71Smutant exhibited a significant heightening in the distance, then gradually decreased, followed by remarkable elevated compared to SHANK3 WT to the end of simulation

time, reflecting an impact on domain interactions and the potential open-up of the SPN-ARR fold over time (**Figure 5.4B**).

The loop structure between SPN and ARR serves as a specific site for the interaction with αCaMKII, which partially conceals the Ras binding site. Recent reports have pointed out the involvement of the linker domain in this loop as a binding surface for αCaMKII. This binding arises in its inactive state, non-phosphorylated, and requires a closed configuration of the SPN-ARR tandem [17, 25]. Consequently, disrupting the connections between SPN and ARR regions may induce a conformational alteration in the Linker domain, leading to lower affinity to αCaMKII. Our findings corresponded with previous results and revealed that the interaction between the SHANK3 WT protein and αCaMKII displayed higher interactions, as indicated in (**Figures 5.5A**, **5.6A**, and **Table 5.1**) compared to the interactions reported in the SHANK3 E71S mutant with αCaMKII, as depicted in (**Figures 5.5B, 5.6B, and Table 5.2**). However, the distinctive interaction between αCaMKII and SHANK3 plays a pivotal role in instigating a specialized long-range signaling pathway from the plasma cell membrane, specifically L-type calcium channels (LTCCs), to the nucleus. This signaling mechanism is imperative for inducing activity-dependent alterations in neuronal gene transcription during the processes of memory and learning [26]. It was claimed the disruption of αCaMKII activity emerges as a prevalent process, generating modifications to the structure of glutamatergic and plasticity neuron function, contributing to the pathogenesis of neurological disorders, including autism [27]. In addition, CaMKIIα is a crucial element in synaptic plasticity, and learning processes play a pivotal role in decoding synaptic Ca2+ oscillations, regulating calcium levels, PSD integration, and shaping the morphology of dendritic spines [25].

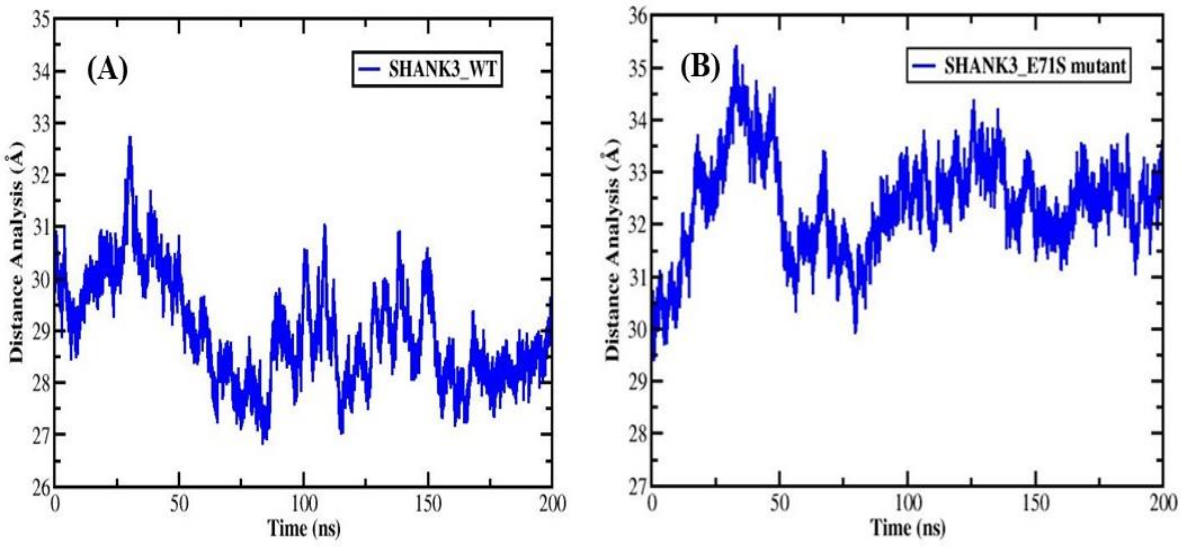

Figure 5.4 *The distance between SPN and ARR domains analysis, (**A**) SHANK3 WT protein, (**B**) SHANK3 E71S mutant.*

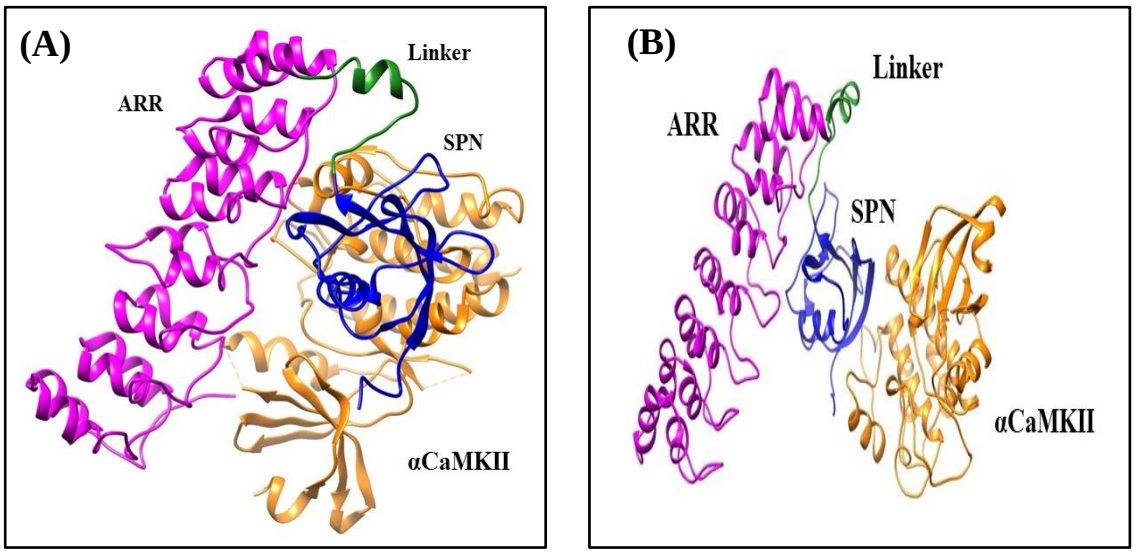

Figure 5.5 *The docking interaction between **(A)** SHANK3 WT protein and αCaMKII, **(B)** SHANK3 E71S mutant and αCaMKII.*

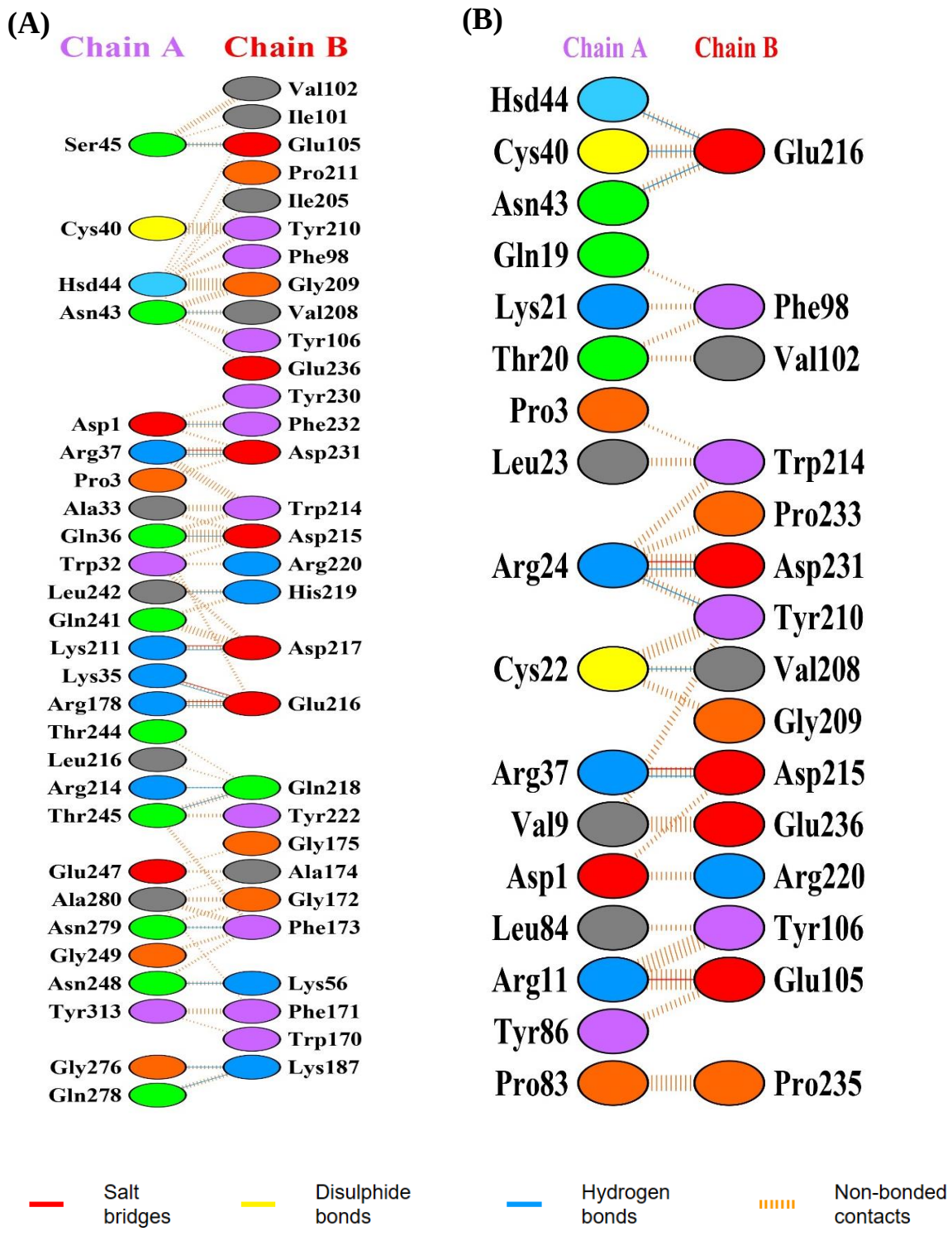

Figure 5.6 *The interactions between* ***(A)*** *SHANK3 WT protein (chain A) with αCaMKII (chain B),* ***(B)*** *SHANK3 E71S mutant (chain A) with αCaMKII (chain B).*

Table 5.1 The interface statistics in SHANK3 WT protein with αCaMKII.

Chain	No. of interface residues	Interface area (A^2)	No. of salt bridges	No. of disulphide bonds	No. of hydrogen bonds	No. of non-bonded contacts
A (SHANK3 WT)	27	1476	4	-	15	202
B (αCaMKII)	30	1448				

Table 5.2 The interface statistics in the SHANK3 E71S mutant αCaMKII.

Chain	No. of interface residues	Interface area (A^2)	No. of salt bridges	No. of disulphide bonds	No. of hydrogen bonds	No. of non-bonded contacts
A (SHANK3 E71S)	17	824	3	-	7	96
B (αCaMKII)	15	862				

5.4.5. Intra-molecular hydrogen bond analysis

Intramolecular hydrogen bonds were assessed to gauge the proximity of all-atom interactions within the SHANK3 WT protein and SHANK3 E71S mutant. These intramolecular hydrogen bond contacts are relevant indicators used for measuring the structural compactness within the distinct domains of the SHANK3 WT protein. The results revealed an increase in intra-molecular interactions in the SHANK3 WT protein in comparison with the SHANK3 E71S mutant, as illustrated in (**Figures 5.7A** and **5.8A**), respectively. Similarly, the SPN domain exhibited higher disparities in the SHANK3 WT protein **(Figure 5.7B)** compared to the SHANK3 E71S mutant (**Figure 5.8B**). Furthermore, no substantial differences in ARR and Linker domains were shown in the SHANK3 WT protein (**Figures 5.7C** and **5.7D**) and SHANK3 E71S mutant, as illustrated in (**Figures 5.8C** and **5.8D**).

Our results indicated that the SHANK3 WT protein has a heightened level of molecular interactions within the SPN, linking to the overall stability of the protein and maintaining a closed conformation, as shown previously in (**Figure 5.3A**). Conversely, the SHANK3 E71S mutant knocked down the intramolecular connections between SPN and ARR, consequently significantly opening up the distance between SPN and ARR regions, as depicted in (**Figure 5.3B)**. Numerous investigations have been initiated to unravel the functional importance of the intramolecular connections between SPN and ARR in SHANK3 [28] and their implications in the pathogenesis of ASD.

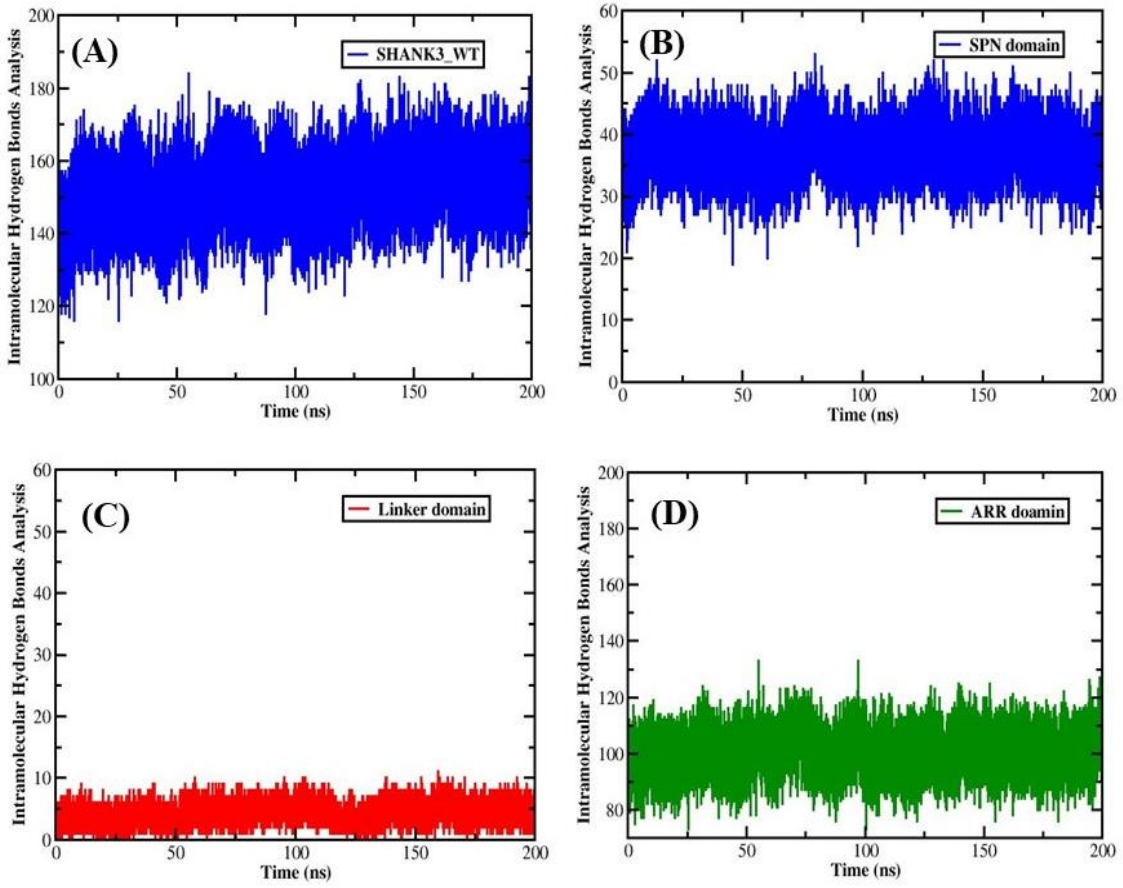

Figure 5.7 *The intramolecular hydrogen bonds analysis, (a) SHANK3 WT protein, (b) SPN domain of SHANK3 WT, (c) Linker domain of SHANK3 WT, (d) ARR domain of SHANK3 WT.*

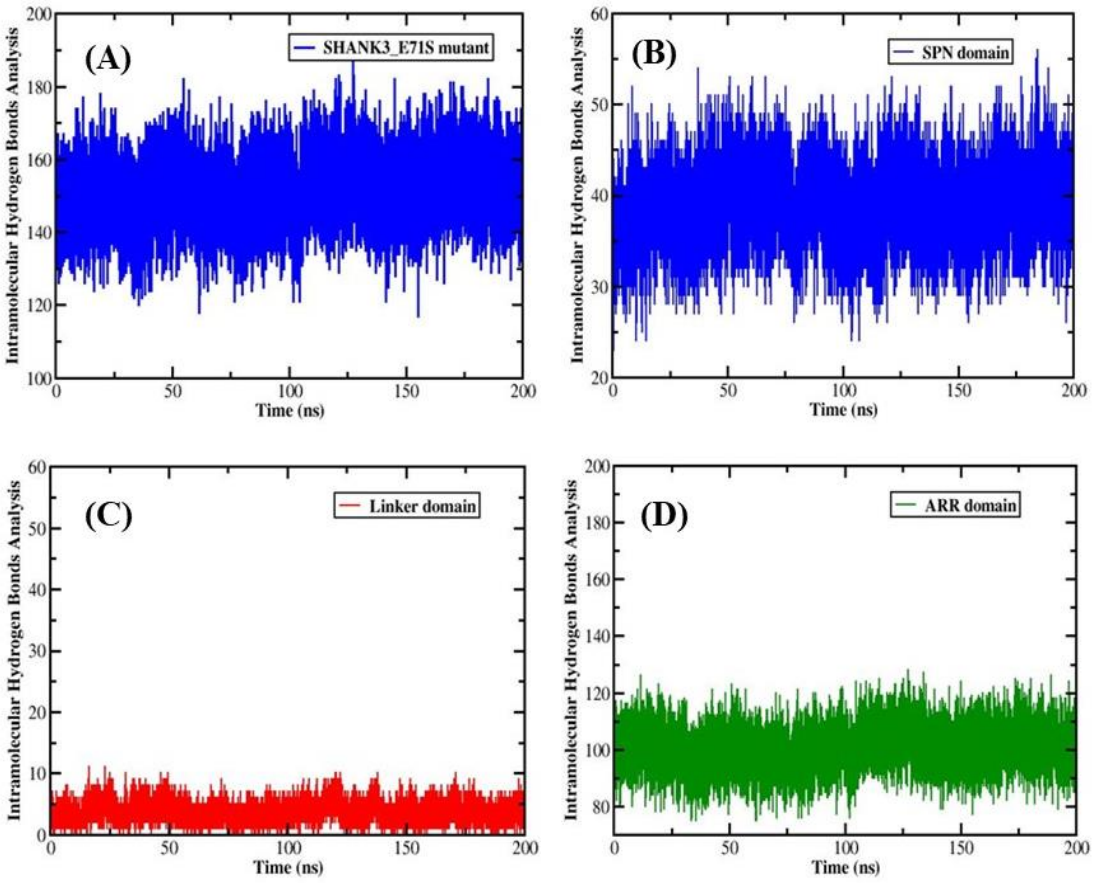

Figure 5.8 *The intramolecular hydrogen bonds analysis, (a) SHANK3 E71S mutant, (b) SPN domain of SHANK3 E71S, (c) Linker domain of SHANK3 E71S, (d) ARR domain of SHANK3 E71S.*

Earlier research indicated that intramolecular interaction prevents α-Fodrin from accessing its location on the ARR domain in SHANK3 WT [29]. However, our findings demonstrated that the SHANK3 E71S mutant disrupted the connections between SPN-ARR domains, so the potential scenario might be that the SHANK3 E71S mutant opens the conformation and facilitates α-Fodrin binding, as shown in (**Tables 5.3** and **5.4**), which increases actin linkage and enhances integrin activation. Taken together, this mutant might change the flexible conformation of SHANK3, impairing the capacity to coordinate cytoskeletal aggregation and signaling dysregulation. The physiological activity of the SHANK3-actin connection influences dendritic protrusion morphology in neuron cells and ASD-related characteristics *in vivo* [16].

Table 5.3 The interface statistics in SHANK3 WT protein with α-Fodrin

Chain	No. of interface residues	Interface area (A^2)	No. of salt bridges	No. of disulphide bonds	No. of hydrogen bonds	No. of non-bonded contacts
A (SHANK3 WT)	15	661	2	-	7	99
B (α-Fodrin)	12	707				

Table 5.4 The interface statistics in the SHANK3 E71S mutant with α-Fodrin

Chain	No. of interface residues	Interface area (A^2)	No. of salt bridges	No. of disulphide bonds	No. of hydrogen bonds	No. of non-bonded contacts
A (SHANK3 E71S)	18	800	5	-	8	125
B (α-Fodrin)	16	852				

5.4.6. Hydrogen bond analysis

The interaction between the SPN and ARR domains was studied through hydrogen bonds. A 200 ns simulation was undertaken for both the SHANK3 WT protein and the SHANK3 E71S mutant to spotlight the specificity of this interaction, a critical aspect of molecular recognition. The analysis targeted residues aa1-92 for the SPN domain and residues aa112-346 for the ARR domain. The findings indicated that the SHANK3 WT protein exhibited more hydrogen bonds than the SHANK3 E71S mutant, as shown in (**Figures 5.9A** and **5.9B**), respectively, indicating more stability.

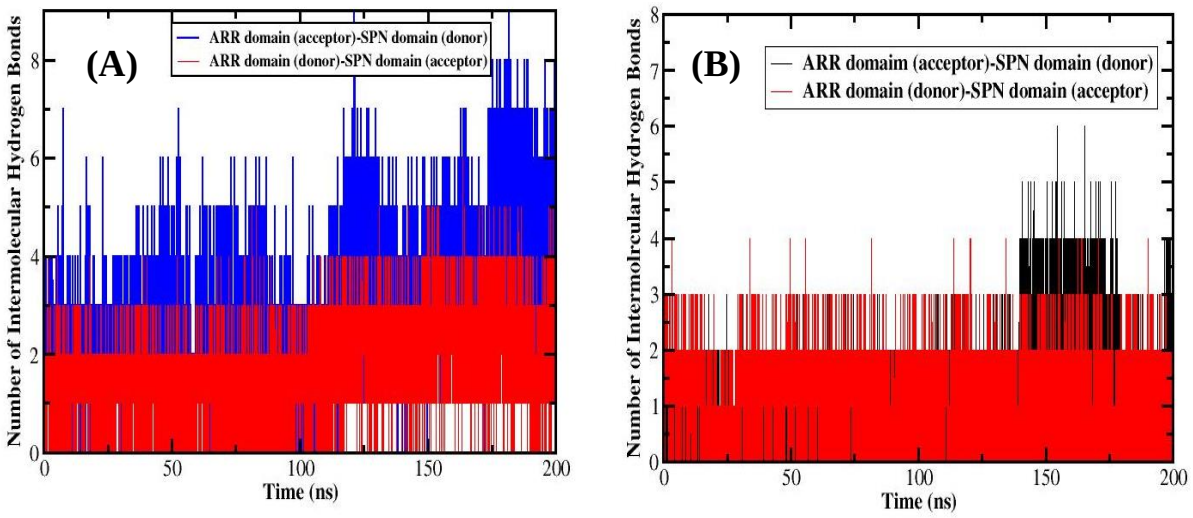

Figure 5.9 *The number of hydrogen bonds between SPN and ARR for 200 ns trajectory, (**A**) SHANK3 WT protein, (**B**) SHANK3 E71S mutant.*

5.4.7. Secondary structure analysis

The secondary structure analysis of the two structures, the SHANK3 WT protein and the SHANK3 E71S mutant were applied. The plots depicting the outcomes for the secondary structure analysis for the SHANK3 WT protein are presented in (**Figures 5.10A-C)** and the SHANK3 E71S mutant, as shown in (**Figures 5.11A-C).** The graphics illustrate the variability of secondary structure across each residue as an indication of frame numbers. We conducted an assessment of the secondary structure probability assumed by the SHANK3 WT and SHANK3 E71S mutant, employing quantitative measures as a function of residue index, as delineated in (**Figures 5.10D-F)** for SHANK3 WT protein, and for SHANK3 E71S mutant (**Figures 5.11D-F)**. In addition, the secondary structure content of the SHANK3 WT protein and the SHANK3 E71S mutant complex have been calculated, it was found that SHANK3 WT has 40.8% helices while SHANK3 E71S mutant has 46.2% helices (**Table 5.5**).

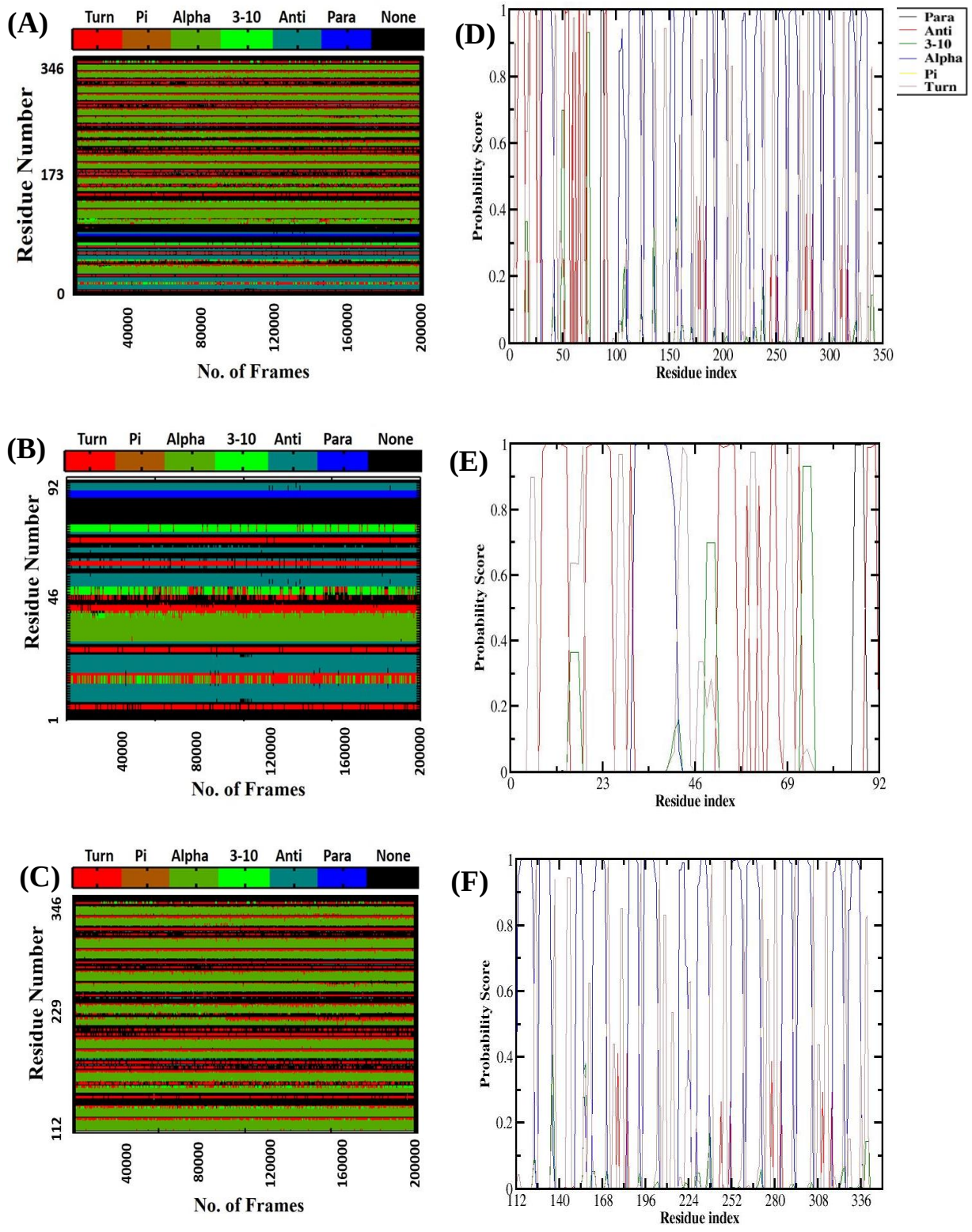

Figure 5.10 *Secondary structure analysis (**A**) SHANK3 WT, (**B**) SPN domain, (**C**) ARR domain. Secondary structure probability score of residue index: (**D**) SHANK3 WT, (**E**) SPN domain, (**F**) ARR domain.*

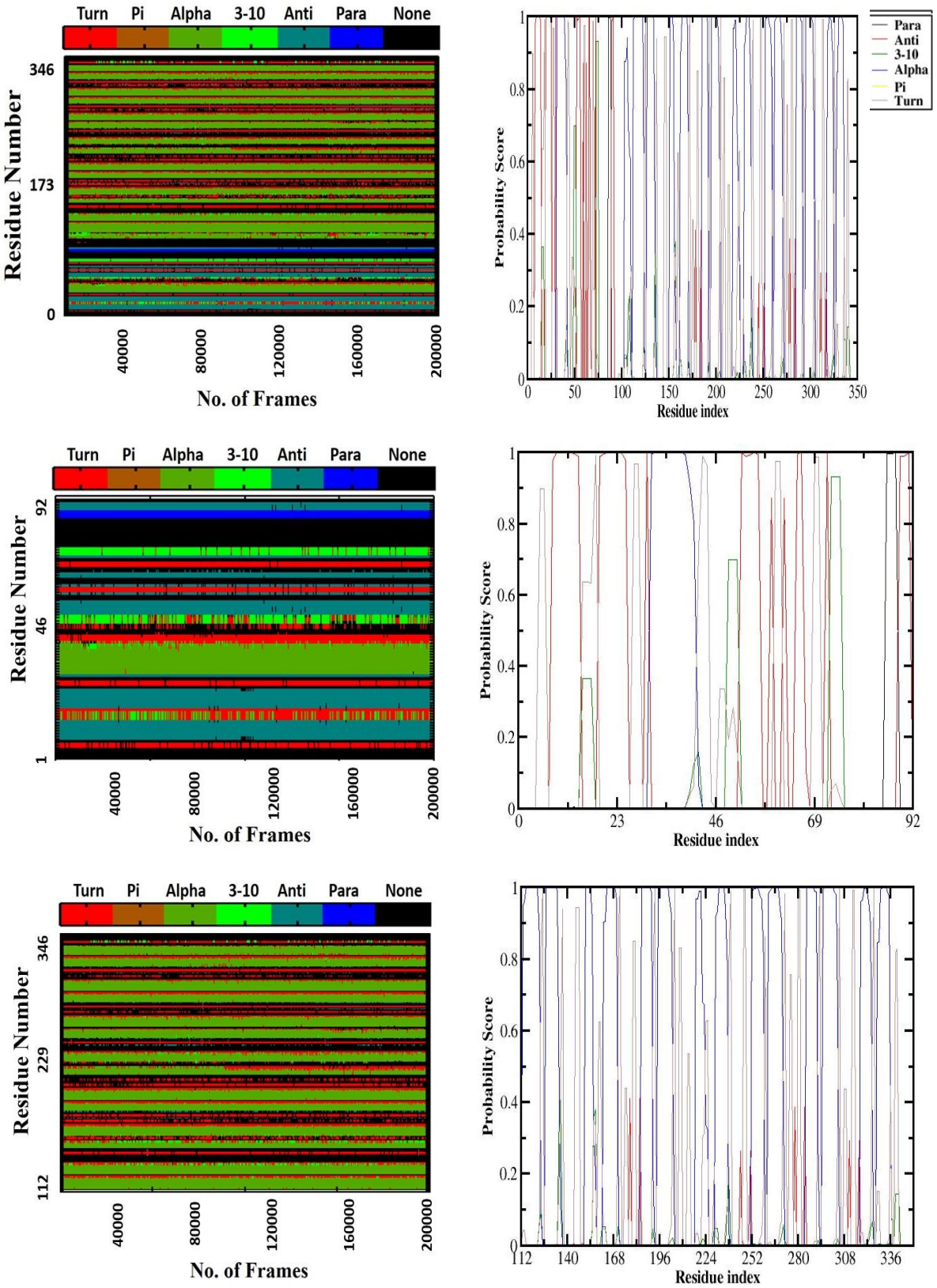

Figure 5.11 *Secondary structure analysis (**A**) SHANK3 E71S mutant, (**B**) SPN domain, (**C**) ARR domain. Secondary structure probability score of residue index: (**D**) SHANK3 E71S mutant, (**E**) SPN domain, (**F**) ARR domain.*

Table 5.5 Secondary structure content in SHANK3 WT protein and SHANK3 E71S mutant.

COMPLEX	**α-helix %**	**β-sheet %**	**turn %**	**Coil %**
SHANK3 WT	40.8	6.9	17.3	35
SHANK3 E71S MUTANT	**46.2**	10	17.3	29

5.5. Conclusion

In summary, our investigation delved extensively into the implications of the SHANK3 E71S mutant, located in the N-terminal region of the SHANK3 gene. The study revealed crucial consequences, notably impeding the stabilization and folding processes of the SHANK3 protein. The SHANK3 E71S mutant disrupted the intramolecular interactions between the SPN and ARR domains, thereby positively influencing its binding with αCaMKII, whereas increased binding α-Fodrin to its sites on the SHANK3. This disruption is anticipated to significantly impact synaptic functionality, potentially contributing to the pathogenesis of ASD. Conversely, the SHANK3 E71S mutant led to a reduction in the binding affinity of α-Fodrin to its site on the ARR domain. These intricate dynamics of SHANK3 mutations, resulting in altered configurations, underscore their potential roles in neurodevelopmental disorders such as ASD. Further studies, both computational and experimental, are warranted to elucidate the precise contributions of this kind of mutation to ASD pathophysiology.

References

[1] Nisar, S. and Haris, M. Neuroimaging genetics approaches to identify new biomarkers for the early diagnosis of autism spectrum disorder. *Molecular psychiatry,* 1-14, 2023. https://doi.org/10.1038/s41380-023-02060-9

[2] Zeidan, J., Fombonne, E., Scorah, J., Ibrahim, A., Durkin, M. S., Saxena, S., Yusuf, A., Shih, A. and Elsabbagh, M. Global prevalence of autism: A systematic review update. *Autism research,* 15: 778-790, 2022. https://doi.org/10.1002/aur.2696

[3] Ghafouri-Fard, S., Pourtavakoli, A., Hussen, B. M., Taheri, M. and Ayatollahi, S. A. A Review on the Role of Genetic Mutations in the Autism Spectrum Disorder. *Molecular Neurobiology,* 60: 5256–5272, 2023. https://doi.org/10.1007/s12035-023-03405-9

[4] Molloy, C. J., Cooke, J., Gatford, N. J., Rivera-Olvera, A., Avazzadeh, S., Homberg, J. R., Grandjean, J., Fernandes, C., Shen, S. and Loth, E. Bridging the translational gap: what can synaptopathies tell us about autism? *Frontiers in Molecular Neuroscience,* 16: 1-20, 2023. https://doi.org/10.3389/fnmol.2023.1191323

[5] Monteiro, P. and Feng, G. SHANK proteins: roles at the synapse and in autism spectrum disorder. *Nature Reviews Neuroscience,* 18: 147-157, 2017. https://doi.org/10.1038/nrn.2016.183

[6] Satterstrom, F. K., Kosmicki, J. A., Wang, J., Breen, M. S., De Rubeis, S., An, J.-Y., Peng, M., Collins, R., Grove, J. and Klei, L. Large-scale exome sequencing study implicates both developmental and functional changes in the neurobiology of autism. *Cell,* 180: 568-584. e23, 2020. https://doi.org/10.1016/j.cell.2019.12.036

[7] Fu, J. M., Satterstrom, F. K., Peng, M., Brand, H., Collins, R. L., Dong, S., Wamsley, B., Klei, L., Wang, L. and Hao, S. P. Rare coding variation provides insight into the genetic architecture and phenotypic context of autism. *Nature genetics,* 54: 1320-1331, 2022. https://doi.org/10.1038/s41588-022-01104-0

[8] Zhou, X., Feliciano, P., Shu, C., Wang, T., Astrovskaya, I., Hall, J. B., Obiajulu, J. U., Wright, J. R., Murali, S. C. and Xu, S. X. Integrating de novo and inherited variants in 42,607 autism cases identifies mutations in new moderate-risk genes. *Nature genetics,* 54: 1305-1319, 2022. https://doi.org/10.1038/s41588-022-01148-2

[9] Cai, Q., Hosokawa, T., Zeng, M., Hayashi, Y. and Zhang, M. Shank3 binds to and stabilizes the active form of Rap1 and HRas GTPases via Its NTD-ANK tandem with distinct mechanisms. *Structure,* 28: 290-300. e4, 2020. https://doi.org/10.1016/j.str.2019.11.018

[10] Hassani Nia, F., Woike, D., Martens, V., Klüssendorf, M., Hönck, H.-H., Harder, S. and Kreienkamp, H.-J. Targeting of δ-catenin to postsynaptic sites through interaction with the Shank3 N-terminus. *Molecular Autism,* 11: 1-17, 2020. https://doi.org/10.1186/s13229-020-00385-8

[11] Chiu, S.-L., Chen, C.-M. and Huganir, R. L. ICA69 regulates activity-dependent synaptic strengthening and learning and memory. *Frontiers in Molecular Neuroscience,* 16: 1-15, 2023. https://doi.org/10.3389/fnmol.2023.1171432

[12] MacGillavry, H. D., Kerr, J. M., Kassner, J., Frost, N. A. and Blanpied, T. A. Shank–cortactin interactions control actin dynamics to maintain flexibility of neuronal spines and synapses. *European Journal of Neuroscience*, 43: 179-193, 2016. https://doi.org/10.1111/ejn.13129

[13] Hassani Nia, F. and Kreienkamp, H.-J. Functional relevance of missense mutations affecting the N-terminal part of Shank3 found in autistic patients. *Frontiers in Molecular Neuroscience*, 11: 1-6, 2018. https://doi.org/10.3389/fnmol.2018.00268

[14] Durand, C. M., Betancur, C., Boeckers, T. M., Bockmann, J., Chaste, P., Fauchereau, F., Nygren, G., Rastam, M., Gillberg, I. C. and Anckarsäter, H. Mutations in the gene encoding the synaptic scaffolding protein SHANK3 are associated with autism spectrum disorders. *Nature genetics*, 39: 25-27, 2007. https://doi.org/10.1038/ng1933

[15] Lilja, J., Zacharchenko, T., Georgiadou, M., Jacquemet, G., Franceschi, N. D., Peuhu, E., Hamidi, H., Pouwels, J., Martens, V. and Nia, F. H. SHANK proteins limit integrin activation by directly interacting with Rap1 and R-Ras. *Nature cell biology*, 19: 292-305, 2017. https://doi.org/10.1038/ncb3487

[16] Salomaa, S. I., Miihkinen, M., Kremneva, E., Paatero, I., Lilja, J., Jacquemet, G., Vuorio, J., Antenucci, L., Kogan, K. and Nia, F. H. SHANK3 conformation regulates direct actin binding and crosstalk with Rap1 signaling. *Current Biology*, 31: 4956-4970, 2021. https://doi.org/10.1016/j.cub.2021.09.022

[17] Woike, D., Wang, E., Tibbe, D., Hassani Nia, F., Failla, A. V., Kibæk, M., Overgård, T. M., Larsen, M. J., Fagerberg, C. R. and Barsukov, I. Mutations affecting the N-terminal domains of SHANK3 point to different pathomechanisms in neurodevelopmental disorders. *Scientific Reports*, 12: 902, 2022. https://doi.org/10.1038/s41598-021-04723-5

[18] Berman, H. M., Westbrook, J., Feng, Z., Gilliland, G., Bhat, T. N., Weissig, H., Shindyalov, I. N. and Bourne, P. E. The protein data bank. *Nucleic acids research*, 28: 235-242, 2000. https://doi.org/10.1093/nar/28.1.235

[19] Pettersen, E. F., Goddard, T. D., Huang, C. C., Couch, G. S., Greenblatt, D. M., Meng, E. C. and Ferrin, T. E. UCSF Chimera—a visualization system for exploratory research and analysis. *Journal of computational chemistry*, 25: 1605-1612, 2004. https://doi.org/10.1002/jcc.20084

[20] Henriques, J., Cragnell, C. and Skepo, M. Molecular dynamics simulations of intrinsically disordered proteins: force field evaluation and comparison with experiment.

Journal of chemical theory computation, 11: 3420-3431, 2015. https://doi.org/10.1021/ct501178z

[21] Jorgensen, W. L., Chandrasekhar, J., Madura, J. D., Impey, R. W. and Klein, M. L. Comparison of simple potential functions for simulating liquid water. *The Journal of chemical physics,* 79: 926-935, 1983. https://doi.org/10.1063/1.445869

[22] Salomon-Ferrer, R., Gotz, A. W., Poole, D., Le Grand, S. and Walker, R. C. Routine microsecond molecular dynamics simulations with AMBER on GPUs. 2. Explicit solvent particle mesh Ewald. *Journal of chemical theory computation,* 9: 3878-3888, 2013. https://doi.org/10.1021/ct400314y

[23] Ryckaert, J.-P., Ciccotti, G. and Berendsen, H. J. Numerical integration of the cartesian equations of motion of a system with constraints: molecular dynamics of n-alkanes. *Journal of computational physics,* 23: 327-341, 1977. https://doi.org/10.1016/0021-9991(77)90098-5

[24] Berendsen, H. J., Postma, J. v., Van Gunsteren, W. F., DiNola, A. and Haak, J. R. Molecular dynamics with coupling to an external bath. *The Journal of chemical physics,* 81: 3684-3690, 1984. https://doi.org/10.1063/1.448118

[25] Cai, Q., Zeng, M., Wu, X., Wu, H., Zhan, Y., Tian, R. and Zhang, M. CaMKIIα-driven, phosphatase-checked postsynaptic plasticity via phase separation. *Cell Research,* 31: 37-51, 2021. https://doi.org/10.1038/s41422-020-00439-9

[26] Perfitt, T. L., Wang, X., Dickerson, M. T., Stephenson, J. R., Nakagawa, T., Jacobson, D. A. and Colbran, R. J. Neuronal L-type calcium channel signaling to the nucleus requires a novel CaMKIIα-Shank3 interaction. *Journal of Neuroscience,* 40: 2000-2014, 2020. https://doi.org/10.1523/JNEUROSCI.0893-19.2020

[27] Robison, A. Emerging role of CaMKII in neuropsychiatric disease. *Trends in neurosciences,* 37: 653-662, 2014. https://doi.org/10.1016/j.tins.2014.07.00

[28] Woike, D., Tibbe, D., Hassani Nia, F., Martens, V., Wang, E., Barsukov, I. and Kreienkamp, H.-J. The Shank/ProSAP N-terminal (SPN) domain of Shank3 regulates targeting to postsynaptic sites and postsynaptic signalling. *bioRxiv,* 1-21, 2023. https://doi.org/10.1101/2023.04.28.538665